

# Reservoir Computing with Diverse Timescales for Prediction of Multiscale Dynamics

Gouhei Tanaka<sup>1,2,3,\*</sup>, Tadayoshi Matsumori<sup>4</sup>, Hiroaki Yoshida<sup>4</sup>, and Kazuyuki Aihara<sup>1</sup>

<sup>1</sup>*International Research Center for Neurointelligence,  
The University of Tokyo, Tokyo 113-0033, Japan*

<sup>2</sup>*Department of Electrical Engineering and Information Systems,*

*Graduate School of Engineering, The University of Tokyo, Tokyo 113-8656, Japan.*

<sup>3</sup>*Department of Mathematical Informatics, Graduate School of Information Science and Technology,*

*The University of Tokyo, Tokyo 113-8656, Japan.*

<sup>4</sup>*Toyota Central Research and Development Laboratory Inc. Tokyo 112-0004, Japan.*

(Dated: August 24, 2021)

Machine learning approaches have recently been leveraged as a substitute or an aid for physical/mathematical modeling approaches to dynamical systems. To develop an efficient machine learning method dedicated to modeling and prediction of multiscale dynamics, we propose a reservoir computing model with diverse timescales by using a recurrent network of heterogeneous leaky integrator neurons. In prediction tasks with fast-slow chaotic dynamical systems including a large gap in timescales of their subsystems dynamics, we demonstrate that the proposed model has a higher potential than the existing standard model and yields a performance comparable to the best one of the standard model even without an optimization of the leak rate parameter. Our analysis reveals that the timescales required for producing each component of target dynamics are appropriately and flexibly selected from the reservoir dynamics by model training.

*Introduction.*— Hierarchical structures composed of macroscale and microscale components are ubiquitous in physical, biological, medical, and engineering systems [1–4]. Complex interactions between such diverse components often bring about multiscale behavior with different spatial and temporal scales. To understand such complex systems, *multiscale modeling* has been one of the major challenges in science and technology [5]. An effective approach is to combine established physical models at different scales by considering their interactions. However, even a physical model focusing on one scale is often not available when the rules (e.g. physical laws) governing the target system are not fully known. In such a case, another potential approach is to employ a machine learning model. Integration of multiscale physical modeling and machine learning techniques is also a practical way under limited knowledge and data [6, 7]. Therefore, it is demanded to develop machine learning models specialized for multiscale dynamics.

We focus on a machine learning framework called *reservoir computing* (RC), which has been mainly applied to temporal pattern recognition such as system identification, time series prediction, time series classification, and anomaly detection [8–13]. The echo state network (ESN) [8, 9], which is a major RC model, uses a recurrent neural network (RNN) to nonlinearly transform an input time series into a high-dimensional dynamic state and reads out desired characteristics from the dynamic state. The RNN with fixed random connection weights serves as a *reservoir* to generate an echo of the past inputs. Compared to other RNNs where all the connection weights are trained with gradient-based learning rules [14], the ESN can be trained with much lower computational cost by optimizing only the readout parameters with a simple learning method [15].

The timescale of reservoir dynamics in the original ESN [8] is almost determined by that of an input time series. However, the timescale of a desired output time series is often largely different from that of the input one depending on a learning task. Therefore, the ESN with leaky integrator neurons (LI-ESN) has been widely used to accommodate the model output to temporal characteristics of the target dynamics [16]. The LI-ESN has a leak rate parameter controlling the update speed of the neuronal states in the reservoir. For multi-timescale dynamics, it is an option to use the hierarchical ESN combining multiple reservoirs with different timescales [17, 18], where the leak rate is common to all the neurons in each reservoir but can be different from one reservoir to another. In all the above models, the leak rate in each reservoir is set at an optimal value through a grid search or a gradient-based optimization.

In contrast to the above approach, here we propose an ESN with diverse timescales (DTS-ESN) where the leak rates of the LI neurons are randomly given. Our aim is to generate reservoir dynamics with a rich variety of timescales so as to produce a wide range of desired time series with different timescales. The main advantage of the DTS-ESN is flexible adjustability to multi-scale dynamics and effortless setting of the leak rates. Moreover, the idea behind the proposed model opens up a possibility to leverage heterogeneous materials and devices with diverse response characteristics for implementing RC hardware [19].

*Methods.*— The DTS-ESN consists of a reservoir with heterogeneous LI neurons and a linear readout as illustrated in Fig. 1(a). The DTS-ESN receives an input time series  $\mathbf{u}(t)$  in the input layer, transforms it into a high-dimensional reservoir state  $\mathbf{x}(t)$ , and produces an output time series  $\mathbf{y}(t)$  as a linear combination of the states

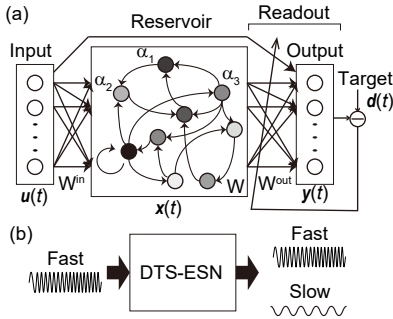


FIG. 1. (a) A schematic of the DTS-ESN. An input time series  $u(t)$  given to the input layer is transformed into a reservoir state  $x(t)$ , and then processed in the readout to produce an output time series  $y(t)$ . Only  $W^{\text{out}}$  is trainable. The reservoir neuron  $i$  has leak rate  $\alpha_i \in [\alpha_{\min}, \alpha_{\max}]$ . (b) A computational task to predict the whole dynamics from only the fast dynamics for a fast-slow dynamical system.

of reservoir neurons. By incorporating a distribution of leak rates of the reservoir neurons, the DTS-ESN extends greatly the range of timescales that can be realized by the LI-ESN [16]. The capability of the DTS-ESN in handling multiscale dynamics is evaluated in a task of predicting the whole dynamics of a fast-slow dynamical system from only its fast dynamics as depicted in Fig. 1(b). An inference of hidden slow dynamics from observational data of the fast dynamics is challenging but beneficial in reducing the effort involved in data measurement. An example in climate science is to predict the slow variables in the deep ocean such as the temperature. They are known to have an important feedback to the fast variables of the atmosphere, land and near-surface oceans [20], but the observation in the deep ocean remains as a major challenge [21]. Prediction of such slow variables can alternatively be made with using the reanalyzed past data for training, which are obtained from the global climate model tuned with data assimilation.

The DTS-ESN is formulated as follows:

$$\mathbf{x}(t + \Delta t) = (\mathbf{1} - \boldsymbol{\alpha})^\top \mathbf{x}(t) + \boldsymbol{\alpha}^\top f(\mathbf{h}(t)), \quad (1)$$

$$\mathbf{h}(t) = \rho W \mathbf{x}(t) + \gamma W^{\text{in}} \mathbf{u}(t + \Delta t), \quad (2)$$

$$\mathbf{y}(t + \Delta t) = W^{\text{out}} [\mathbf{x}(t + \Delta t); \mathbf{u}(t + \Delta t); 1], \quad (3)$$

where  $t$  is the time,  $\Delta t$  is the time step,  $\mathbf{x}(t) \in \mathbb{R}^{N_x}$  is the reservoir state vector,  $\mathbf{1} \in \mathbb{R}^{N_x}$  in Eq. (1) is the all-ones vector,  $\boldsymbol{\alpha} = (\alpha_1, \dots, \alpha_{N_x})^\top$  is the vector of leak rates,  $\mathbf{h}(t)$  is the internal state vector,  $f$  is an element-wise activation function,  $\rho W \in \mathbb{R}^{N_x \times N_x}$  is the reservoir weight matrix with spectral radius  $\rho$ ,  $\gamma W^{\text{in}} \in \mathbb{R}^{N_x \times N_u}$  is the input weight matrix with input scaling factor  $\gamma$ ,  $\mathbf{u}(t) \in \mathbb{R}^{N_u}$  is the input vector,  $\mathbf{y}(t) \in \mathbb{R}^{N_y}$  is the output vector,  $W^{\text{out}} \in \mathbb{R}^{N_y \times (N_x + N_u + 1)}$  is the output weight matrix, and the symbol “;” means a vertical concatenation of the vectors. Only  $W^{\text{out}}$  is trainable and all the other parameters are fixed in advance [8, 12].

In this study, the activation function was given by the hyperbolic tangent (i.e.  $f = \tanh$ ). The entries of  $W^{\text{in}}$  were randomly drawn from a uniform distribution in  $[-1, 1]$ . The connection density of the random recurrent network as a reservoir was set at  $d = 0.1$ , which represents the fraction of non-zero entries of  $W$ . The non-zero entries were randomly drawn from a uniform distribution in  $[-1, 1]$  and rescaled so that the spectral radius of  $W$  equals 1. As for the leak rates,  $\log_{10} \alpha_i$  was randomly drawn from a uniform distribution in  $[\log_{10} \alpha_{\min}, \log_{10} \alpha_{\max}]$  to generate largely different timescales of the reservoir dynamics. We note that  $\alpha_i \in [\alpha_{\min}, \alpha_{\max}]$  follows a reciprocal (or log-uniform) distribution. The leak rate  $\alpha_i$  of neuron  $i$  is represented as  $\alpha_i = \Delta t / c_i$  where  $c_i$  denotes the time constant in the corresponding continuous-time model (see the Supplemental Material [22]). In the training phase, an optimal output weight matrix  $\hat{W}^{\text{out}}$  is obtained with ridge regression where the following sum of squared output errors plus the regularization term is minimized:

$$\sum_{k=k_{\min}}^{k_{\max}} \|\mathbf{y}(t + k\Delta t) - \mathbf{d}(t + k\Delta t)\|_2^2 + \beta \|W^{\text{out}}\|_F^2, \quad (4)$$

where  $[k_{\min}\Delta t, k_{\max}\Delta t]$  represents the training period,  $\|\cdot\|_2$  indicates the L2 norm,  $\|\cdot\|_F$  indicates the Frobenius norm,  $\mathbf{d}(t)$  denotes the target dynamics, and  $\beta$  represents the regularization factor [12]. In the testing phase,  $\hat{W}^{\text{out}}$  is used to produce predicted outputs from unseen input time series data. The DTS-ESN is reduced to the LI-ESN [16] when  $\alpha_i = \alpha$  for  $i = 1, \dots, N_x$ .

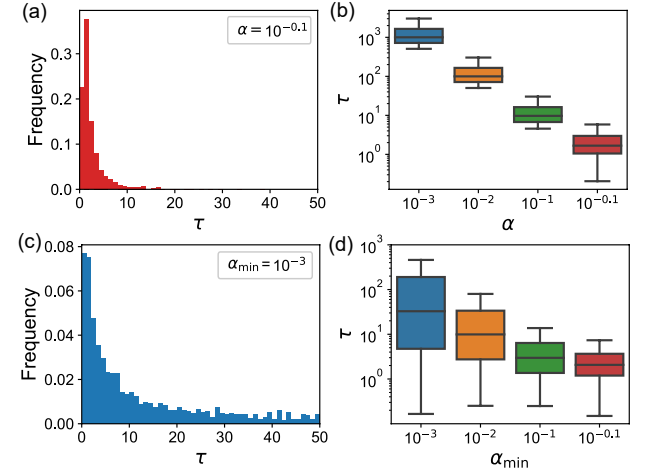


FIG. 2. Timescale distributions of reservoir dynamics in the linearized systems of the LI-ESN and the DTS-ESN when  $N_x = 2000$  and  $d = 0.1$ . (a) A histogram of timescales ( $\tau_i$ ) in Eq. (5)) in the LI-ESN with  $\alpha = 10^{-0.1}$ . (b) The effect of  $\alpha$  on the timescale distribution in the LI-ESN. (c) The same as (a) but in the DTS-ESN with  $\alpha_{\max} = 1$  and  $\alpha_{\min} = 10^{-3}$ . (d) The effect of  $\alpha_{\min}$  on the timescale distribution in the DTS-ESN with  $\alpha_{\max} = 1$ .

TABLE I. Fast-slow chaotic dynamical systems models used for prediction tasks. Each model consists of fast and slow subsystems of the variables specified in the third and fourth columns. The parameter values were set to exhibit chaotic dynamics.

Model names	Equations	Fast	Slow	Parameter values
(i) Rulkov [23]	$x_{n+1} = \eta/(1+x_n^2) + y_n, y_{n+1} = y_n - \mu(x_n - \sigma)$	$x$	$y$	$\eta = 4.2, \mu = 0.001, \sigma = -1.0$
(ii) Hindmarsh-Rose [24]	$\dot{x} = y - x^3 + bx^2 - z + I, \dot{y} = 1 - 5x^2 - y, \dot{z} = \epsilon(s(x - x_0) - z)$	$x, y$	$z$	$b = 3.05, I = 3, \epsilon = 0.01, s = 4, x_0 = -1.6$
(iii) tc-VdP [25]	$\dot{x}_1 = (y_1 + c_1 x_2)/\tau_1, \dot{y}_1 = (\mu_1(1 - x_1^2)y_1 - x_1)/\tau_1 \\ \dot{x}_2 = (y_2 + c_2 x_1)/\tau_2, \dot{y}_2 = (\mu_2(1 - x_2^2)y_2 - x_2)/\tau_2$	$x_1, y_1$	$x_2, y_2$	$\mu_1 = 5, \tau_1 = 0.1, c_1 = 0.001 \\ \mu_2 = 5, \tau_2 = 1, c_2 = 1$
(iv) tc-Lorenz [26]	$\dot{X} = a(Y - X), \dot{Y} = r_s x - ZX - Y - \epsilon_s xy, \dot{Z} = XY - bZ, \dot{x} = ca(y - x), \dot{y} = c(r_f x - zx - y) + \epsilon_f Yx, \dot{z} = c(xy - bz)$	$x, y, z$	$X, Y, Z$	$a = 10, b = 8/3, c = 10 \\ r_s = 28, r_f = 45, \epsilon_s = 0.01, \epsilon_f = 10$

*Analyses.*— The timescales of the reservoir dynamics in the DTS-ESN are determined by the hyperparameters including the time step  $\Delta t$ , the spectral radius  $\rho$ , and the leak rate vector  $\alpha$ . The timescales of reservoir dynamics in the linearized system of Eq. (1), denoted by  $\tau_i$  for  $i = 1, \dots, N_x$ , are linked to the set of eigenvalues  $\lambda_i$  of its Jacobian matrix as follows (see the Supplemental Material [22]):

$$\tau_i = -\frac{\Delta t}{\ln |\lambda_i|}. \quad (5)$$

Figure 2 demonstrates that the timescale distribution in the linearized system is different between the LI-ESN and the DTS-ESN. Figure 2(a) shows a timescale distribution for the LI-ESN with  $\alpha = 10^{-0.1}$ . When  $\alpha$  is decreased to produce slower dynamics, the peak of the timescale distribution increases while the distribution range in the logarithmic scale is almost unaffected as shown in Fig. 2(b) [18]. Figure 2(c) shows a broader timescale distribution of the DTS-ESN with  $[\alpha_{\min}, \alpha_{\max}] = [10^{-3}, 1]$ . As shown in Fig. 2(d), the distribution range monotonically increases with a decrease in  $\alpha_{\min}$  (see the Supplemental Material [22]). The timescale analysis based on the linearized systems indicates that the DTS-ESN with a sufficiently small  $\alpha_{\min}$  has much more diverse timescales than the LI-ESN.

*Results.*— We evaluated the computational performance of the DTS-ESN in time series prediction tasks with four fast-slow chaotic dynamical systems models listed in Table I: (i) the Rulkov model which is a 2D map replicating chaotic bursts of neurons [23]; (ii) the Hindmarsh-Rose (HR) model which is a phenomenological neuron model exhibiting irregular spiking-bursting behavior [24]; (iii) the two coupled Van der Pol (tc-VdP) model which is a combination of fast and slow limit cycle oscillators with nonlinear damping [25]; (iv) the two coupled Lorenz (tc-Lorenz) model which is a caricature representing the interaction of the ocean with slow dynamics and the atmosphere with fast dynamics [26, 27]. There is a large timescale gap between the fast and slow subsystems in the above models. From these models, we generated time series data for training and testing (see the Supplemental Material [22]). We consider a one-step-ahead prediction

where the states of the whole variables at one step ahead are predicted from the input time series of only the fast variables (see Fig. 1(b)). The prediction performance is evaluated with the Normalized Root Mean Squared Error (NRMSE) between the model output and the target output, defined as follows:

$$\text{NRMSE} = \frac{\sqrt{\langle \|\mathbf{y}(t + k\Delta t) - \mathbf{d}(t + k\Delta t)\|_2^2 \rangle_k}}{\sqrt{\langle \|\mathbf{d}(t + k\Delta t) - \langle \mathbf{d}(t + k\Delta t) \rangle_k \|_2^2 \rangle_k}}, \quad (6)$$

where  $\langle \cdot \rangle_k$  represents an average over the total time steps.

Figure 3 demonstrates a one-step-ahead prediction with the DTS-ESN for the tc-Lorenz model. Figure 3(a) shows the histogram of  $\log_{10} \alpha_i$  generated randomly from a uniform distribution in [-3,0]. Due to the presence of diverse timescales in the reservoir of the DTS-ESN, not only the fast dynamics ( $x, y$ , and  $z$ ) but also the slow dynamics ( $X, Y$ , and  $Z$ ) is well predicted as shown in

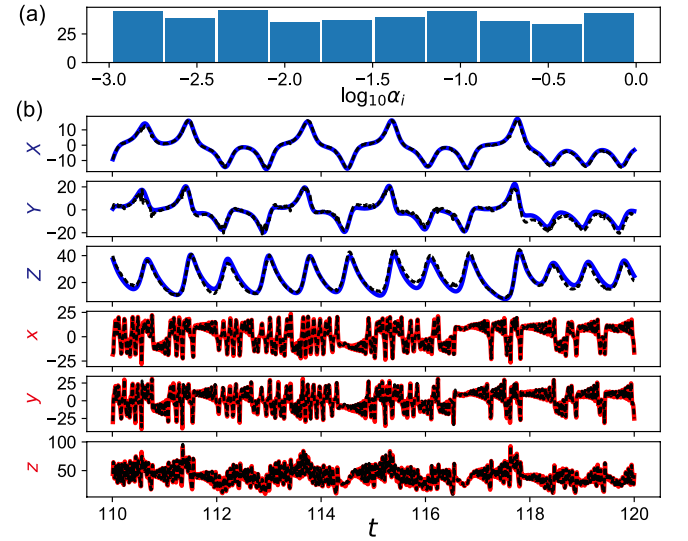


FIG. 3. A prediction for the tc-Lorenz model using the trained DTS-ESN where  $N_u = 3, N_x = 400, N_y = 6, d = 0.1, \gamma = 0.1, \rho = 0.1, \beta = 10^{-3}, \alpha_{\max} = 1$ , and  $\alpha_{\min} = 10^{-3}$ . The inputs are the fast dynamics ( $x, y$ , and  $z$ ) and the outputs are the whole dynamics ( $X, Y, Z, x, y$ , and  $z$ ). (a) The histogram of  $\log_{10} \alpha_i$ . (b) Model predictions (black dashed lines) and the target time series (red: fast, blue: slow).

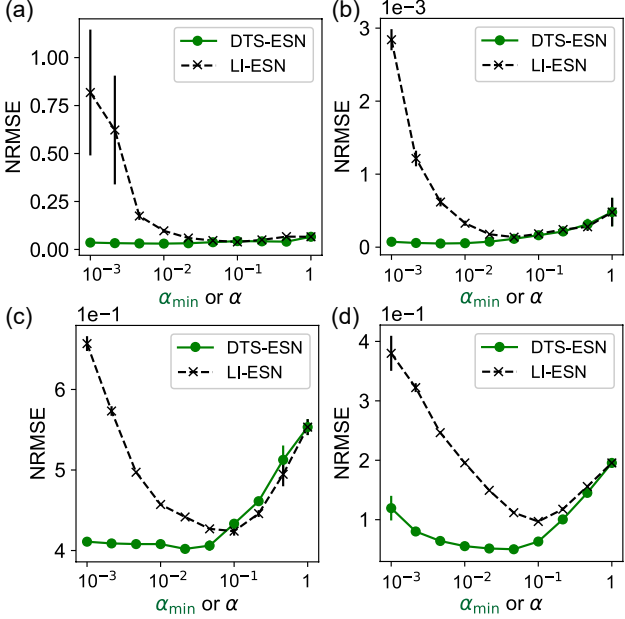


FIG. 4. Comparisons of the testing errors (NRMSE) between the DTS-ESN (green circles) and the LI-ESN (black crosses). The marks indicate the average errors over ten simulation runs with different reservoir realizations, and the error bar indicates the variance. (a) The Rulkov model. (b) The Hindmarsh-Rose model. (c) The tc-VdP model. (d) The tc-Lorenz model.

Fig. 3(b) (see the Supplemental Material for the results for the other systems in Table I [22]). Once the DTS-ESN is trained with the teacher data on the whole dynamics, it can be used to infer the unobserved hidden states from the observational data of the fast variables owing to the interactions between the fast and slow subsystems.

Figures 4(a)-(d) show the comparisons between the DTS-ESN and the LI-ESN in the prediction performance for the four dynamical systems models listed in Table I. The horizontal axis is  $\alpha_{\min}$  for the DTS-ESN and  $\alpha$  for the LI-ESN. When  $\alpha_{\min} = \alpha = 1$ , the two models coincide and yield the same performance. The prediction performance is improved as  $\alpha_{\min}$  is decreased from 1 for the DTS-ESN, mainly due to an increase in the prediction accuracy with respect to the slow variables (see the Supplemental Material [22]). The DTS-ESN can keep a relatively small prediction error when  $\alpha_{\min}$  is decreased even to  $10^{-3}$  in contrast to the LI-ESN. The best performance of the DTS-ESN is better than that of the LI-ESN for all the target dynamical systems, indicating a higher ability of the DTS-ESN. Moreover, if we set  $\alpha_{\min} = 10^{-3}$  to ensure sufficiently diverse timescales, the DTS-ESN can achieve the performance comparable to the best one achieved by the LI-ESN for all the target dynamics. This effortless setting of leak rates is an advantage of the DTS-ESN over the LI-ESN and its variants.

Figures 5(a)-(d) visualize the output weight matrix

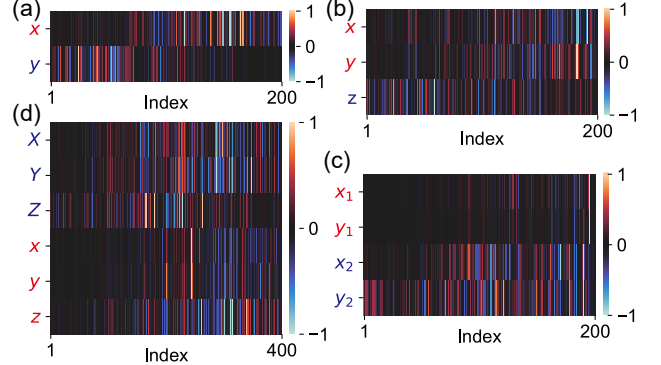


FIG. 5. The output weight matrix  $\hat{W}^{\text{out}}$  in trained DTS-ESNs. The vertical axis indicates the state variables (red: fast, blue: slow) in the target dynamical systems. The horizontal axis indicates the indices of reservoir neurons sorted in the ascending order of leak rate  $\alpha_i$ . (a) The Rulkov model. (b) The Hindmarsh-Rose model. (c) The tc-VdP model. (d) The tc-Lorenz model.

$\hat{W}^{\text{out}}$  obtained by training the DTS-ESN for the four dynamical systems models. Note that the last  $(N_u + 1)$  columns corresponding to the connections from the input layer and the bias were eliminated. The indices of reservoir neurons were sorted in the ascending order of leak rate  $\alpha_i$ . The matrix elements with relatively large absolute values are indicated by colors other than black, corresponding to the reservoir neurons that are mainly used for producing each component of the target dynamics. We can see that the neuronal states with appropriate timescales are selected to comply with the timescale of the desired output as a result of model training. In Fig. 5(d) for the tc-Lorenz model, the reservoir neurons with very small  $\alpha_i$  are used for the slow variable  $Z$  but not for the other slow variables,  $X$  and  $Y$ . This means that the dynamics of  $X$  and  $Y$  are essentially not as slow as that of  $Z$ , leading to the performance degradation with a large decrease in  $\alpha_{\min}$  as shown in Fig. 4(d).

*Discussion and conclusion.*— We have proposed the RC model with diverse timescales, the DTS-ESN, by incorporating distributed leak rates into the reservoir neurons for modeling and prediction of multiscale dynamics. The results of the prediction tasks indicate the effectiveness of our randomization approach to realizing a reservoir with rich timescales. Although we assumed a specific distribution of leak rates, another distribution could further improve the prediction performance. Moreover, another type of heterogeneity of reservoir components could boost the ability of RC systems in approximating a wide variety of dynamical systems. Future applications include a prediction of large-scale spatiotemporal chaotic systems [13, 28] from partial observations and an inference of slow dynamics from experimentally measured data involved in real-world multiscale systems [21, 29].

We thank Daisuke Inoue for fruitful discussion. This work was performed as a project of Intelligent Mobility Society Design, Social Cooperation Program (Next Generation Artificial Intelligence Research Center, the University of Tokyo with Toyota Central R&D Labs., Inc.), and supported in part by JSPS KAKENHI Grant Number 20K11882 (GT), JST-Mirai Program Grant Number JPMJMI19B1 (GT), JST CREST Grant Number JPMJCR19K2 (GT), JST Moonshot R&D Grant Number JPMJMS2021 (KA), AMED under Grant Number JP21dm0307009 (KA), UTokyo Center for Integrative Science of Human Behavior (CiSHuB) (KA), and International Research Center for Neurointelligence at The University of Tokyo Institutes for Advanced Study (UTIAS) (GT, KA).

- 
- [1] D. G. Vlachos, A review of multiscale analysis: examples from systems biology, materials engineering, and other fluid–surface interacting systems, *Advances in Chemical Engineering* **30**, 1 (2005).
- [2] K. Matouš, M. G. Geers, V. G. Kouznetsova, and A. Gillman, A review of predictive nonlinear theories for multiscale modeling of heterogeneous materials, *Journal of Computational Physics* **330**, 192 (2017).
- [3] T. S. Deisboeck, Z. Wang, P. Macklin, and V. Cristini, Multiscale cancer modeling, *Annual Review of Biomedical Engineering* **13**, 127 (2011).
- [4] J. Walpole, J. A. Papin, and S. M. Peirce, Multiscale computational models of complex biological systems, *Annual Review of Biomedical Engineering* **15**, 137 (2013).
- [5] E. Weinan, *Principles of multiscale modeling* (Cambridge University Press, 2011).
- [6] J. Pathak, A. Wikner, R. Fussell, S. Chandra, B. R. Hunt, M. Girvan, and E. Ott, Hybrid forecasting of chaotic processes: Using machine learning in conjunction with a knowledge-based model, *Chaos: An Interdisciplinary Journal of Nonlinear Science* **28**, 041101 (2018).
- [7] M. Alber, A. B. Tepole, W. R. Cannon, S. De, S. Duran-Bernal, K. Garikipati, G. Karniadakis, W. W. Lytton, P. Perdikaris, L. Petzold, *et al.*, Integrating machine learning and multiscale modeling-perspectives, challenges, and opportunities in the biological, biomedical, and behavioral sciences, *npj Digital Medicine* **2**, 1 (2019).
- [8] H. Jaeger, The “echo state” approach to analysing and training recurrent neural networks-with an erratum note, Bonn, Germany: German National Research Center for Information Technology GMD Technical Report **148**, 13 (2001).
- [9] H. Jaeger and H. Haas, Harnessing nonlinearity: Predicting chaotic systems and saving energy in wireless communication, *Science* **304**, 78 (2004).
- [10] W. Maass, T. Natschläger, and H. Markram, Real-time computing without stable states: A new framework for neural computation based on perturbations, *Neural Computation* **14**, 2531 (2002).
- [11] D. Verstraeten, B. Schrauwen, M. d’Haene, and D. Stroobandt, An experimental unification of reservoir computing methods, *Neural Networks* **20**, 391 (2007).
- [12] M. Lukoševičius and H. Jaeger, Reservoir computing approaches to recurrent neural network training, *Computer Science Review* **3**, 127 (2009).
- [13] J. Pathak, B. Hunt, M. Girvan, Z. Lu, and E. Ott, Model-free prediction of large spatiotemporally chaotic systems from data: A reservoir computing approach, *Physical Review Letters* **120**, 024102 (2018).
- [14] P. J. Werbos, Backpropagation through time: what it does and how to do it, *Proceedings of the IEEE* **78**, 1550 (1990).
- [15] M. Lukoševičius, A practical guide to applying echo state networks, in *Neural networks: Tricks of the trade* (Springer, 2012) pp. 659–686.
- [16] H. Jaeger, M. Lukoševičius, D. Popovici, and U. Siebert, Optimization and applications of echo state networks with leaky-integrator neurons, *Neural Networks* **20**, 335 (2007).
- [17] H. Jaeger, *Discovering multiscale dynamical features with hierarchical echo state networks*, Tech. Rep. (Jacobs University Bremen, 2007).
- [18] L. Manneschi, M. O. Ellis, G. Gigante, A. C. Lin, P. Del Giudice, and E. Vasilaki, Exploiting multiple timescales in hierarchical echo state networks, *Frontiers in Applied Mathematics and Statistics* **6**, 76 (2021).
- [19] G. Tanaka, T. Yamane, J. B. Héroux, R. Nakane, N. Kanazawa, S. Takeda, H. Numata, D. Nakano, and A. Hirose, Recent advances in physical reservoir computing: A review, *Neural Networks* **115**, 100 (2019).
- [20] A. K. Seshadri, Fast–slow climate dynamics and peak global warming, *Climate Dynamics* **48**, 2235 (2017).
- [21] C. S. Meinen, R. C. Perez, S. Dong, A. R. Piola, and E. Campos, Observed ocean bottom temperature variability at four sites in the northwestern argentine basin: evidence of decadal deep/abyssal warming amidst hourly to interannual variability during 2009–2019, *Geophysical Research Letters* **47**, e2020GL089093 (2020).
- [22] See supplementary material at [URL will be inserted by publisher] for further details.
- [23] N. F. Rulkov, Regularization of synchronized chaotic bursts, *Physical Review Letters* **86**, 183 (2001).
- [24] J. L. Hindmarsh and R. Rose, A model of neuronal bursting using three coupled first order differential equations, *Proceedings of the Royal Society of London. Series B. Biological Sciences* **221**, 87 (1984).
- [25] K. P. Champion, S. L. Brunton, and J. N. Kutz, Discovery of nonlinear multiscale systems: Sampling strategies and embeddings, *SIAM Journal on Applied Dynamical Systems* **18**, 312 (2019).
- [26] G. Boffetta, P. Giuliani, G. Paladin, and A. Vulpiani, An extension of the Lyapunov analysis for the predictability problem, *Journal of the Atmospheric Sciences* **55**, 3409 (1998).
- [27] F. Borra, A. Vulpiani, and M. Cencini, Effective models and predictability of chaotic multiscale systems via machine learning, *Physical Review E* **102**, 052203 (2020).
- [28] P. R. Vlachas, J. Pathak, B. R. Hunt, T. P. Sapsis, M. Girvan, E. Ott, and P. Koumoutsakos, Backpropagation algorithms and reservoir computing in recurrent neural networks for the forecasting of complex spatiotemporal dynamics, *Neural Networks* **126**, 191 (2020).
- [29] T. Proix, V. K. Jirsa, F. Bartolomei, M. Guye, and W. Truccolo, Predicting the spatiotemporal diversity of seizure propagation and termination in human focal

epilepsy, *Nature Communications* **9**, 1 (2018).

**Supplemental Material:  
Reservoir Computing with Diverse Timescales for Prediction of  
Multiscale Dynamics**

Gouhei Tanaka<sup>1,2,3,\*</sup>, Tadayoshi Matsumori<sup>4</sup>, Hiroaki Yoshida<sup>4</sup>, and Kazuyuki Aihara<sup>1</sup>

<sup>1</sup>*International Research Center for Neurointelligence,  
The University of Tokyo, Tokyo 113-0033, Japan*

<sup>2</sup>*Department of Electrical Engineering and Information Systems,  
Graduate School of Engineering, The University of Tokyo, Tokyo 113-8656, Japan.*

<sup>3</sup>*Department of Mathematical Informatics,  
Graduate School of Information Science and Technology,  
The University of Tokyo, Tokyo 113-8656, Japan.*

<sup>4</sup>*Toyota Central Research and Development Laboratory Inc. Tokyo, Japan.*

## I. DERIVATION OF THE DTS-ESN

The continuous-time system corresponding to the update of reservoir states in the DTS-ESN (see Eq. (1) in the main text) is described as follows:

$$c_i \frac{dx_i(t)}{dt} = -x_i(t) + f(h_i(t)) \quad \text{for } i = 1, \dots, N_x, \quad (1)$$

where  $x_i(t)$  is the  $i$ -th component of the reservoir state vector  $\mathbf{x}(t)$ ,  $h_i(t)$  is the  $i$ -th component of the internal state vector  $\mathbf{h}(t) = \rho W \mathbf{x}(t) + \gamma W^{\text{in}} \mathbf{u}(t)$ , and  $c_i$  is the coefficient scaling the time constant for neuron  $i$  in the reservoir. The DTS-ESN is derived by discretizing the above model in time using the Euler method in a similar way to the derivation of the LI-ESN [1]. By applying the Euler discretization with time step  $\Delta t$ , i.e.

$$\frac{dx_i(t)}{dt} \approx \frac{x_i(t + \Delta t) - x_i(t)}{\Delta t}, \quad (2)$$

we can rewrite Eq. (1) as follows:

$$x_i(t + \Delta t) = \left(1 - \frac{\Delta t}{c_i}\right) x_i(t) + \frac{\Delta t}{c_i} f(h_i(t)) \quad \text{for } i = 1, \dots, N_x. \quad (3)$$

By defining the leak rate as  $\alpha_i \equiv \Delta t/c_i$ , we obtain the following equation:

$$x_i(t + \Delta t) = (1 - \alpha_i) x_i(t) + \alpha_i f(h_i(t)) \quad \text{for } i = 1, \dots, N_x. \quad (4)$$

This is equivalent to Eq. (1) in the main text, described as follows:

$$\mathbf{x}(t + \Delta t) = (\mathbf{1} - \boldsymbol{\alpha})^\top \mathbf{x}(t) + \boldsymbol{\alpha}^\top f(\mathbf{h}(t)), \quad (5)$$

where  $\boldsymbol{\alpha} = (\alpha_1, \dots, \alpha_{N_x})^\top$ .

## II. TIMESCALES AND EIGENVALUES

### II-A. Timescales of linearized systems

The time evolution of the reservoir state in the DTS-ESN is described as Eq. (5). By linearizing Eq. (5) at the fixed point at the origin, we obtain a linearized dynamical system as follows:

$$\mathbf{x}(t + \Delta t) = J \mathbf{x}(t), \quad (6)$$

where  $J$  is the Jacobian matrix. Note that the linearized system of the LI-ESN can also be described in the above form. Assuming that  $J$  is diagonalizable, we have the following equation:

$$P^{-1}JP = \Lambda, \quad (7)$$

where  $\Lambda = \text{diag}(\lambda_1, \dots, \lambda_{N_x})$  is a diagonal matrix composed of the eigenvalues of  $J$ , and  $P$  is a matrix composed of the corresponding eigenvectors. By defining  $\mathbf{x} = P\mathbf{y}(t)$ , we can rewrite Eq. (6) as follows:

$$\mathbf{y}(t + \Delta t) = \Lambda \mathbf{y}(t), \quad (8)$$

which is a set of independent  $N_x$  linear difference equations. The solution of the  $i$ -th equation is given by

$$\begin{aligned} y_i(t) &= \lambda_i^{t/\Delta t} y_i(0) \\ &= |\lambda_i|^{t/\Delta t} (\cos((t/\Delta t)\theta_i) + j \sin((t/\Delta t)\theta_i)) y_i(0), \end{aligned} \quad (9)$$

where  $\text{Re}(\lambda_i) = |\lambda_i| \cos \theta_i$  and  $\text{Im}(\lambda_i) = |\lambda_i| \sin \theta_i$ . Since  $|\lambda_i|^{t/\Delta t} = e^{(t/\Delta t) \ln |\lambda_i|}$ , the exponential decay rate with regard to neuron  $i$  in the reservoir is expressed as follows:

$$t/\tau_i = -(t/\Delta t) \ln |\lambda_i|, \quad (10)$$

where  $\tau_i$  is the timescale of the dynamics of neuron  $i$  in the reservoir. Hence, we have Eq. (5) in the main text as follows:

$$\tau_i = -\frac{\Delta t}{\ln |\lambda_i|}. \quad (11)$$

## II-B. Difference between DTS-ESN and LI-ESN

The distribution of timescales realized by the DTS-ESN is largely different from that by the LI-ESN (see Figure 2 in the main text). Here we observe their difference in terms of the eigenvalue distribution of the Jacobian matrix.

The Jacobian matrix of the linearized system of the LI-ESN is given by

$$J_L = I - \alpha I + \rho \alpha W, \quad (12)$$

where  $\alpha$  is the leak rate common to all the reservoir neurons,  $W$  is the recurrent weight matrix of the reservoir, and  $\rho$  is the spectral radius of  $\rho W$ . Since  $W$  is scaled so that

its spectral radius (i.e. the maximum absolute eigenvalue) is unity, the eigenvalues of  $W$ , denoted by  $\lambda_i^{(W)}$  ( $i = 1, \dots, N_x$ ), are uniformly distributed over the unit disk on the complex plane. The eigenvalues of  $J_L$ , denoted by  $\lambda_i^{(J_L)}$ , can be described as follows [2]:

$$\lambda_i^{(J_L)} = 1 - \alpha + \rho\alpha\lambda_i^{(W)} \quad \text{for } i = 1, \dots, N_x. \quad (13)$$

The distribution of these eigenvalues for different  $\alpha$  values are shown in Fig. S1(a). The eigenvalue distribution is a circular uniform distribution over a circle with radius  $\rho\alpha$ , centered at  $1 - \alpha$ . When  $\rho = 1$ , the original circular distribution at  $\alpha = 1$  (solid curve) drastically shrinks with a decrease in the  $\alpha$  value, and eventually all the eigenvalues converge to 1 on the real axis in the limit of  $\alpha \rightarrow 0$ . The leak rate  $\alpha$  has a role to restrict the range of timescales as shown in Fig. 2 in the main text, because both the maximum and minimum values of  $-1/\ln|\lambda_i^{(J_L)}|$  (see Eq. (11)) monotonically increases as  $\alpha$  is decreased.

On the other hand, the Jacobian matrix of the linearized system of the DTS-ESN is given by

$$J_D = I - A + \rho AW, \quad (14)$$

where  $A = \text{diag}(\alpha_1, \dots, \alpha_{N_x})$  is the diagonal matrix of leak rates of the neurons in the reservoir. The  $(i, j)$  entry of  $J_D$  is given by  $1 - \alpha_i + \rho\alpha_i w_{ij}$ . Since both  $\alpha_i$  and  $w_{ij}$  are randomly generated,  $J_D$  can be viewed as a random matrix. The distribution of the eigenvalues of  $J_D$ , denoted by  $\lambda_i^{(J_D)}$ , is shown in Fig. S1(b). When  $\alpha_{\min}$  is decreased from 1, the range of

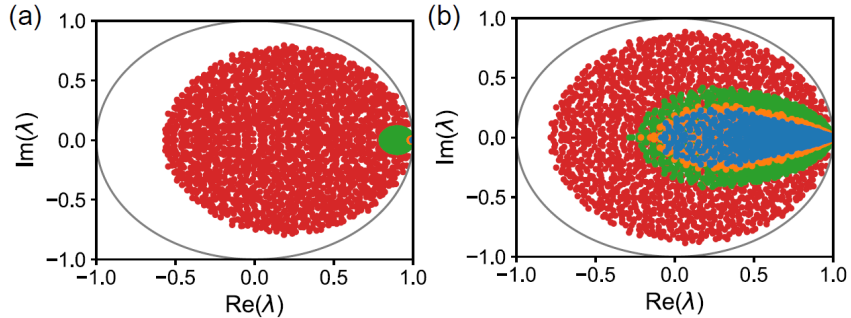


FIG. S1. Distributions of eigenvalues of the Jacobian matrices. The parameter values were set at  $N_x = 2000$ ,  $d = 0.1$ ,  $\rho = 1$ , and  $\Delta t = 1$ . (a) LI-ESN. The leak rate  $\alpha$  was set at  $10^{-0.1}$  (red),  $10^{-1}$  (green),  $10^{-2}$  (orange), and  $10^{-3}$  (blue). (b) DTS-ESN with  $\alpha_{\max} = 1$ . The value of  $\alpha_{\min}$ , was set at  $10^{-0.1}$  (red),  $10^{-1}$  (green),  $10^{-2}$  (orange), and  $10^{-3}$  (blue).

the eigenvalue distribution shrinks and the maximum value of  $-1/\ln |\lambda_i^{(J_D)}|$  monotonically increases. We notice that the eigenvalues close to the origin (i.e. those with small  $|\lambda_i^{(J_D)}|$ ) remain owing to the random distribution of  $\alpha_i$ . As a result, the diverse timescales can be realized in the DTS-ESN (see Fig. 2 in the main text).

If the eigenvalue distribution of  $J_D$  is analytically derived, the probabilistic distribution function of the timescales in the DTS-ESN could be obtained. We have explored this possibility based on the random matrix theory, but it is still under investigation.

### III. DATASETS FOR PREDICTION TASKS

As described in the main text, we consider a one-step-ahead prediction where the states of the whole variables at one step ahead are predicted from the input time series of only the fast variables (see Fig. 1(b) in the main text). In the prediction tasks, the time series datasets were generated from the four chaotic fast-slow dynamical systems listed in Table I of the main text. For the Rulkov model (see (i) in Table I), the time series data was obtained by updating the states in the difference equations. For the other models (see (ii)-(iv) in Table I), the time series data was obtained by numerically integrating the ordinary differential equations using the fourth-order Runge-Kutta method with time step  $\Delta t$  (see Table S1 below). The initial condition of each state variable was randomly given from a uniform distribution in  $[0,1]$  for all the models. The data lengths for transient, training, testing, and total periods are listed in Table S1. The data in the transient periods, influenced by the initial conditions, were discarded. We have trained the machine learning models using the dataset in the training periods. Then, by setting the trained  $\hat{W}^{\text{out}}$ , we generated predicted outputs using the dataset in the testing periods.

TABLE S1. Datasets for prediction tasks. The 2nd column corresponds to the time step and the 3rd-6th columns correspond to the data lengths.

Model names	Time step	Transient	Training	Testing	Total
(i) Rulkov [3]	$(\Delta t = 1)$	4000	8000	4000	16000
(ii) Hindmarsh-Rose [4]	$\Delta t = 0.05$	$200/\Delta t = 4000$	$1200/\Delta t = 24000$	$600/\Delta t = 12000$	$2000/\Delta t = 40000$
(iii) tc-VdP [5]	$\Delta t = 0.01$	$50/\Delta t = 5000$	$150/\Delta t = 15000$	$100/\Delta t = 10000$	$300/\Delta t = 30000$
(iv) tc-Lorenz [6]	$\Delta t = 0.01$	$30/\Delta t = 3000$	$60/\Delta t = 6000$	$30/\Delta t = 3000$	$120/\Delta t = 12000$

#### IV. EXAMPLES OF PREDICTIONS

Figure S2(a)-(c) demonstrate the examples of predictions with the DTS-ESN for the Rulkov model, the Hindmarsh-Rose model, and the tc-VdP model, respectively. The top panel shows the histogram of leak rates, which is the same as Fig. 3(a) in the main text and identical to all the examples.

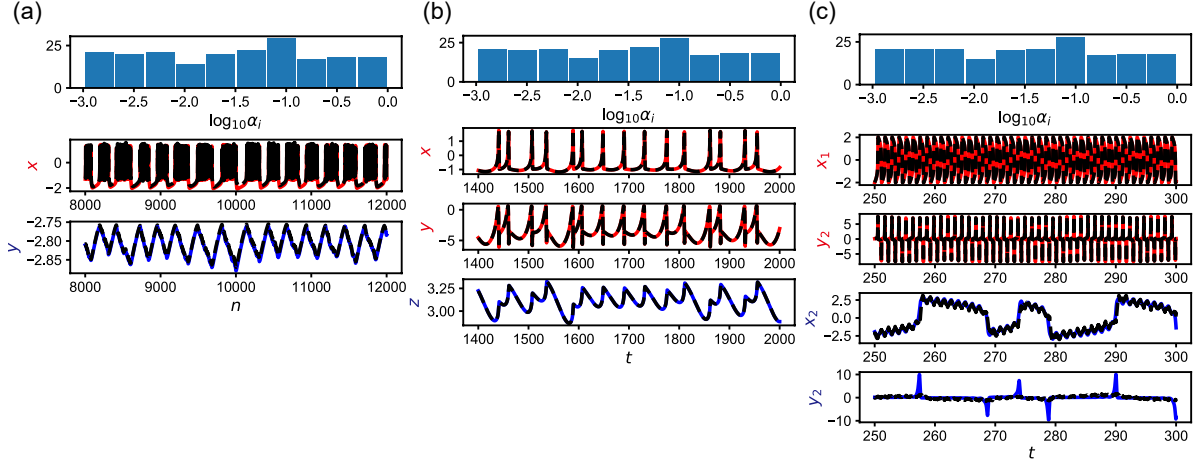


FIG. S2. Examples of time series prediction with the DTS-ESN. The top panel shows the histogram of  $\log_{10} \alpha_i$ . The target time series is indicated by solid lines (red: fast, blue: slow). The predictive output is indicated by the black dashed lines. The parameter values were set at  $N_x = 200$ ,  $d = 0.1$ ,  $\gamma = 1$ ,  $\rho = 1$ ,  $\beta = 10^{-3}$ ,  $\alpha_{\max} = 1$ , and  $\alpha_{\min} = 10^{-3}$ . (a) The Rulkov model.  $N_u = 1$  and  $N_y = 2$ . (b) The Hindmarsh-Rose model.  $N_u = 2$  and  $N_y = 3$  (c) The tc-VdP model.  $N_u = 2$  and  $N_y = 4$ .

#### V. PARAMETER DEPENDENCE OF THE PREDICTION PERFORMANCE

Figures S3 shows the comparisons between the DTS-ESN and the LI-ESN in prediction errors (NRMSE) for each variable when  $\alpha_{\min}$  in the DTS-ESN and  $\alpha$  in the LI-ESN are varied. The panels with label ‘All’ correspond to the cases with all the variables as in Fig. 4 in the main text. Note that the ‘All’ panels in Figs. S3(a) and (b) are enlargements of Figs. 4(a) and (b) in the main text, respectively. Since the timescale is different depending on the variable, the optimal value of  $\alpha$  achieving the minimum NRMSE is also different

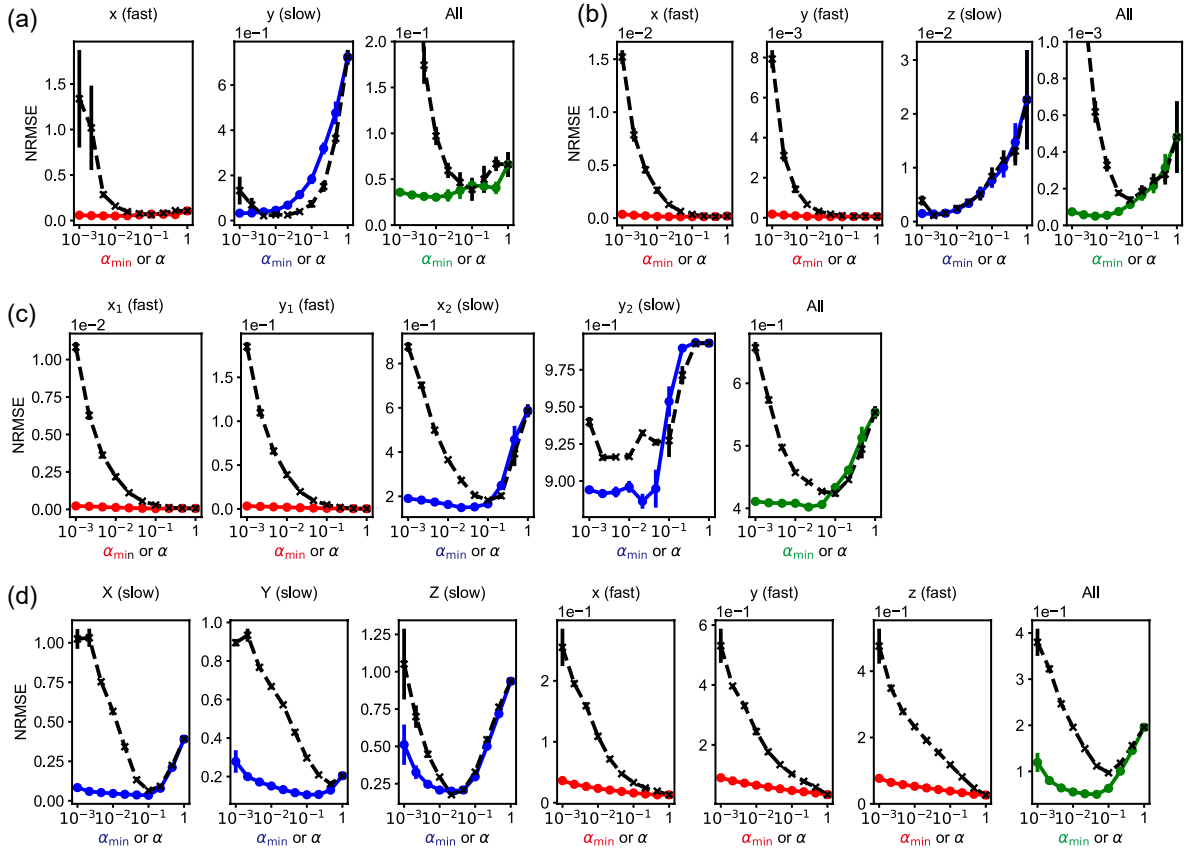


FIG. S3. Comparisons between the DTS-ESN (circles) and the LI-ESN (crosses) in the prediction tasks. The performance was evaluated with NRMSE in the vertical axis. The horizontal axis is  $\alpha_{\min}$  for the DTS-ESN and  $\alpha$  for the LI-ESN. The red, blue, and green colors correspond to the fast, slow, and whole variables, respectively. (a) The Rulkov model.  $N_x = 200$  and  $\rho = \gamma = 1$ . (b) The Hindmarsh-Rose model.  $N_x = 200$  and  $\rho = \gamma = 1$ . (c) The tc-VdP model.  $N_x = 200$  and  $\rho = \gamma = 1$ . (d) The tc-Lorenz model.  $N_x = 400$  and  $\rho = \gamma = 0.1$ .

between the variables. In the LI-ESN, this gap in the appropriate  $\alpha$  values makes it difficult to hold down the total error. In the DTS-ESN, the  $\alpha_i$  values that are suited for the timescale of each variable are naturally selected as a result of model training. Thus, the diversity of timescales in the DTS-ESN is advantageous in handling multiscale dynamics.

The dependence of the prediction result on the input scaling parameter  $\gamma$  (in addition to the leak rate parameters) is shown in Fig. S4. The dependence of the prediction result on the spectral radius  $\rho$  (in addition to the leak rate parameters) is shown in Fig. S5. By comparing the upper and lower panels for each variable of each dynamical system model, we

can see that the DTS-ESN totally yields better performance than the LI-ESN. Through these parameter variations, we found that relatively good performance is obtained at  $\rho = \gamma = 1$  for the Rulkov model, the Hindmarsh-Rose model, and the tc-VdP model, and at  $\rho = \gamma = 0.1$  for the tc-Lorenz model. Therefore, we set the two parameters,  $\rho$  and  $\gamma$ , at these values in Figs. 4 and 5 in the main text.

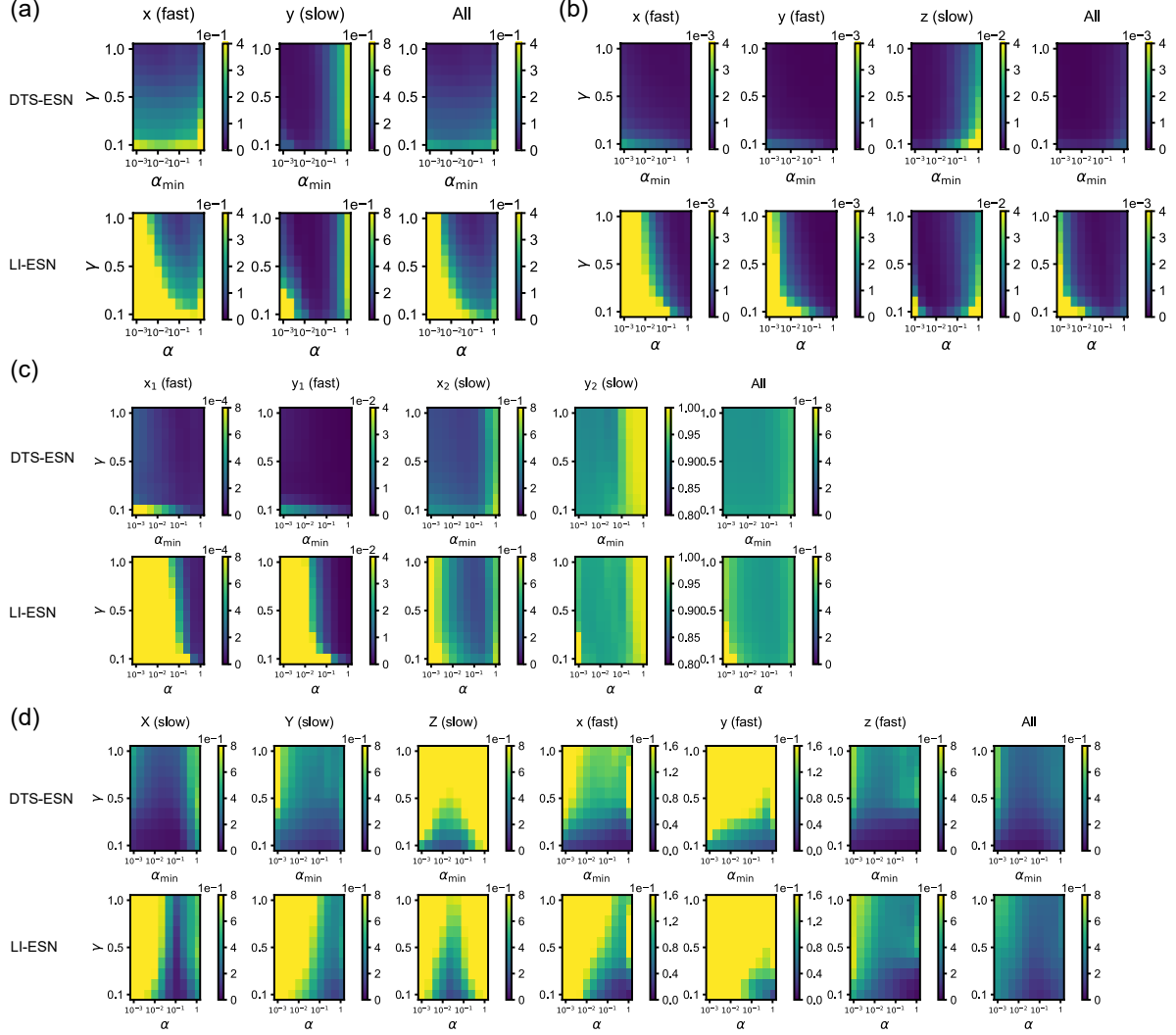


FIG. S4. Comparisons between the DTS-ESN (upper panels) and the LI-ESN (lower panels) in the prediction performance. The predictive performance was evaluated with NRMSE indicated by the color on the  $(\alpha_{\min}, \gamma)$  plane for the DTS-ESN and on the  $(\alpha, \gamma)$  plane for the LI-ESN. (a) The Rulkov model.  $N_x = 200$  and  $\rho = 1$ . (b) The Hindmarsh-Rose model.  $N_x = 200$  and  $\rho = 1$ . (c) The tc-VdP model.  $N_x = 200$  and  $\rho = 1$ . (d) The tc-Lorenz model.  $N_x = 400$  and  $\rho = 0.1$ .

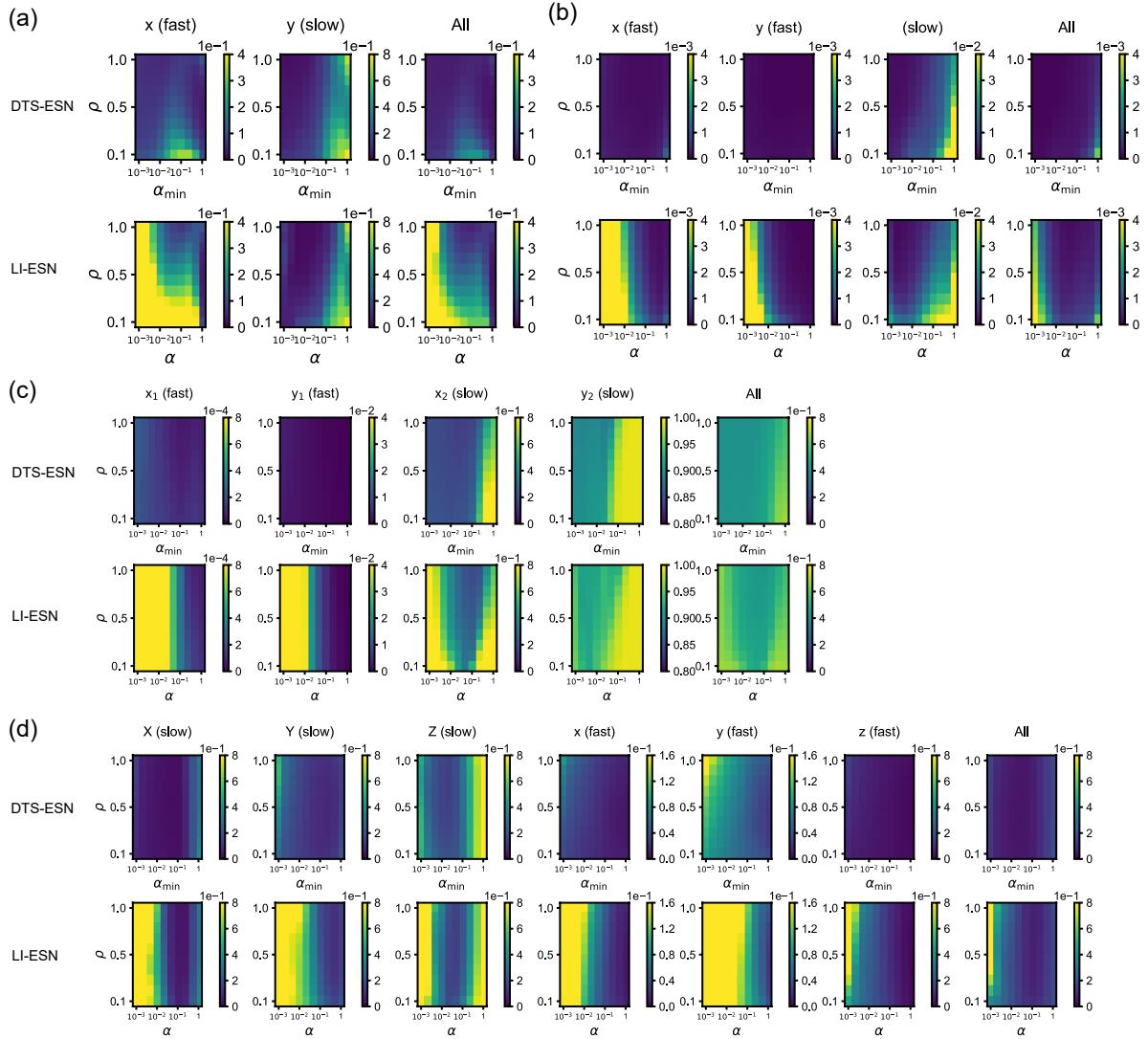


FIG. S5. Comparisons between the DTS-ESN (upper panels) and the LI-ESN (lower panels) in the prediction performance. The prediction performance was evaluated with NRMSE indicated by the color on the  $(\alpha_{\min}, \rho)$  plane for the DTS-ESN and on the  $(\alpha, \rho)$  plane for the LI-ESN. (a) The Rulkov model.  $N_x = 200$  and  $\gamma = 1$ . (b) The Hindmarsh-Rose model.  $N_x = 200$  and  $\gamma = 1$ . (c) The tc-VdP model.  $N_x = 200$  and  $\gamma = 1$ . (d) The tc-Lorenz model.  $N_x = 400$  and  $\gamma = 0.1$ .

- 
- [1] H. Jaeger, M. Lukoševičius, D. Popovici, and U. Siewert, Optimization and applications of echo state networks with leaky-integrator neurons, *Neural Networks* **20**, 335 (2007).
  - [2] L. Manneschi, M. O. Ellis, G. Gigante, A. C. Lin, P. Del Giudice, and E. Vasilaki, Exploiting multiple timescales in hierarchical echo state networks, *Frontiers in Applied Mathematics and Statistics* **6**, 76 (2021).
  - [3] N. F. Rulkov, Regularization of synchronized chaotic bursts, *Physical Review Letters* **86**, 183 (2001).
  - [4] J. L. Hindmarsh and R. Rose, A model of neuronal bursting using three coupled first order differential equations, *Proceedings of the Royal Society of London. Series B. Biological Sciences* **221**, 87 (1984).
  - [5] K. P. Champion, S. L. Brunton, and J. N. Kutz, Discovery of nonlinear multiscale systems: Sampling strategies and embeddings, *SIAM Journal on Applied Dynamical Systems* **18**, 312 (2019).
  - [6] G. Boffetta, P. Giuliani, G. Paladin, and A. Vulpiani, An extension of the Lyapunov analysis for the predictability problem, *Journal of the Atmospheric Sciences* **55**, 3409 (1998).